International Journal of Multiphase Flow 105 (2018) 84–90

Contents lists available at ScienceDirect

International Journal of Multiphase Flow

journal homepage: www.elsevier.com/locate/ijmulflow

Phase-field simulation of Rayleigh instability on a fibre

Junxiang Yang[a], Junseok Kim[a,1,*]

Department of Mathematics, Korea University, Seoul 02841, Republic of Korea

ARTICLE INFO

Article history:
Received 28 November 2017
Revised 23 March 2018
Accepted 23 March 2018
Available online 28 March 2018

Keywords:
Cahn–Hilliard equation
Navier–Stokes equation
Rayleigh instability
Unconditionally stable scheme
Flow on a fibre

ABSTRACT

In this paper, we present a phase-field method for Rayleigh instability on a fibre. Unlike a liquid column, the evolutionary dynamics of a liquid layer on a fibre depends on the boundary condition at the solid-liquid interface. We use a Navier–Stokes–Cahn–Hilliard system to model axisymmetric immiscible and incompressible two-phase flow with surface tension on a fibre. We solve the Navier–Stokes equation using a projection method and the Cahn–Hilliard equation using a nonlinearly stable splitting method. We present computational experiments with various thicknesses of liquid thread and fibre. The numerical results indicate that the size of the satellite droplet decreases as the thicknesses of the thread and fibre increase.

1. Introduction

The coating problem of a cylindrical fibre with a liquid film has been intensively studied because of its relation with technological and industrial processes, i.e., the coating of conducting cables with isolating films (González et al., 2010). However, compared to a lot of literature on the simulations of the break-up of a liquid thread under the Rayleigh instability (RI) (Chakrabarti et al., 2017; Gopan and Sarith, 2014; Joshi et al., 2016; Vega et al., 2010; Yan et al., 2015) and references therein, there are only few numerical works on the RI on a fibre (González et al., 2010; Haefner et al., 2015; Mead-Hunter et al., 2012). Fig. 1 shows optical micrographs illustrating the temporal evolutions of the Plateau–Rayleigh instability for a liquid polystyrene film on a glass fibre (Haefner et al., 2015).

Using a lubrication approximation, the authors in Haefner et al. (2015) obtained a governing equation for the one-dimensional axisymmetric surface profile over time and compared with various experiments. In particular, they reported on the RI dynamics with two different boundary conditions on the liquid and fibre. The breakup of a liquid film coating a fiber into an array of droplets was simulated using a three-dimensional volume-of-fluid method by the authors in Mead-Hunter et al. (2012). They also compared the numerical results with experimental observations and existing theory. The instability of a liquid film coating a thin cylindrical fibre was investigated numerically and experimentally by González et al. (2010). They reported experimental results such as growth rates and dominant wavelengths of the interface. They also presented direct numerical simulations and compared with the experimental data.

In this work, we will use a phase-field method for the Rayleigh instability on a fibre and investigate the effects of the thickness of the liquid film and the fibre on the evolution dynamics. The phase-field method is popular in modeling two-phase fluid flows. For example, Bai et al. (2017) used a 3D phase-field model to simulate the droplet formation process in a flow-focusing device. There are other numerical methods for multiphase fluid flows such as the level-set method (Rodríguez, 2017) and the volume-of-fluid method (Müller et al., 2016).

The outline of the paper is as follows. The phase-field model in cylindrical coordinates is presented in Section 2. The numerical solution is given in Section 3. The proposed numerical schemes are tested in Section 4. Finally, conclusions are derived in Section 5.

2. Axisymmetric Navier–Stokes–Cahn–Hilliard system

We consider the two-phase fluid consisting of two components, fluid 1 and fluid 2, on a solid fibre. We denote by ϕ the composition difference of the mixture of two fluids. The phase-field ϕ is a normalized concentration and its value is equal to $+1$ and -1 when the two phases are at mutual equilibrium. In this study, we focus on density matched case. The axisymmetric Navier–Stokes–Cahn–Hilliard system (Kim, 2005b) is

$$\nabla \cdot \mathbf{u} = 0, \tag{1}$$

$$\rho(\mathbf{u}_t + \mathbf{u} \cdot \nabla \mathbf{u}) = -\nabla p + \nabla \cdot [\eta(\phi)(\nabla \mathbf{u} + \nabla \mathbf{u}^T)] + \mathbf{SF}(\phi), \tag{2}$$

$$\phi_t + \nabla \cdot (\phi \mathbf{u}) = M \Delta \mu, \tag{3}$$

* Corresponding author.
E-mail address: cfdkim@korea.ac.kr (J. Kim).
[1] http://math.korea.ac.kr/~cfdkim.

https://doi.org/10.1016/j.ijmultiphaseflow.2018.03.019
0301-9322/

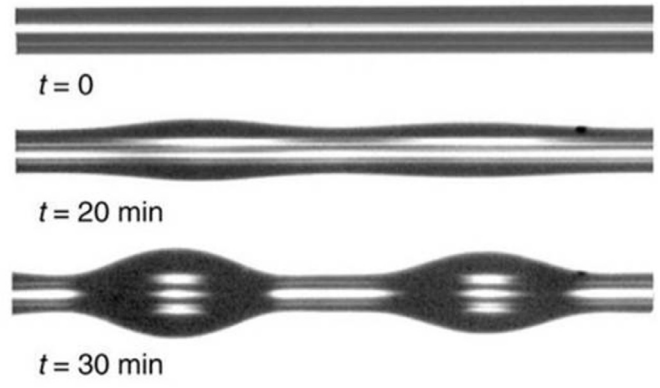

Fig. 1. Plateau–Rayleigh instability for a liquid polystyrene film on a glass fibre. Adapted from Haefner et al. (2015) with permission from Nature Publishing Group.

$$\mu = \alpha\phi^3 - \beta\phi - \kappa\Delta\phi, \tag{4}$$

where $\mathbf{u}$ the velocity, ρ is the density, p the pressure, and $\eta(\phi) = \eta_1(1+\phi)/2 + \eta_2(1-\phi)/2$ is the variable viscosity, where η_1 and η_2 are viscosity coefficients of fluid 1 and 2, respectively. The surface tension force (Kim, 2005a) is

$$\mathbf{SF}(\phi) = -\frac{3\sqrt{2}\sigma\epsilon}{4}\nabla\cdot\left(\frac{\nabla\phi}{|\nabla\phi|}\right)|\nabla\phi|\nabla\phi, \tag{5}$$

where σ is the interfacial tension coefficient and ϵ is the small positive parameter related to interfacial transition thickness. Other thermodynamically consistent surface tension force, i.e., the Korteweg force can be found in Kim (2005a) and Lamorgese et al. (2017), M is the positive mobility, and α, β, κ are constant. μ is the generalized (i.e., including its non-local part) chemical potential difference near the critical point. Eqs. (1)–(5) couple each other through concentration-dependent viscosity and surface tension force, and the advection for the phase-field ϕ. If we nondimensionalize the governing Eqs. (1)–(4), then we have

$$\nabla\cdot\mathbf{u} = 0, \tag{6}$$

$$\mathbf{u}_t + \mathbf{u}\cdot\nabla\mathbf{u} = -\nabla p + \frac{1}{Re}\nabla\cdot[\eta(\phi)(\nabla\mathbf{u} + \nabla\mathbf{u}^T)] + \frac{1}{We}\mathbf{SF}(\phi), \tag{7}$$

$$\phi_t + \nabla\cdot(\phi\mathbf{u}) = \frac{1}{Pe}\Delta\mu, \tag{8}$$

$$\mu = \phi^3 - \phi - \epsilon^2\Delta\phi, \tag{9}$$

where we set $\alpha, \beta = 1$, $\kappa = \epsilon^2$ and the Reynolds, Weber, and Peclet numbers are given by $Re = \rho_c U_c L_c/\eta_c$, $We = \rho_c L_c U_c^2/\sigma_c$, and $Pe = U_c L_c/(M_c\mu_c)$ using characteristic values, respectively. More details about the nondimensionalization can be found in Kim (2005b) and Lee et al. (2011). Because we are interested in axisymmetric Navier–Stokes–Cahn–Hilliard system for the cylindrical viscous liquid thread on a solid fibre, we rewrite Eqs. (6)–(9) in axisymmetric form:

$$\frac{1}{r}(ru)_r + w_z = 0, \tag{10}$$

$$u_t + uu_r + wu_z = -p_r + \frac{SF^r}{We} + \frac{1}{Re}\left(\frac{1}{r}(r(2\eta u_r))_r + (\eta(w_r+u_z))_z - \frac{2\eta u}{r^2}\right), \tag{11}$$

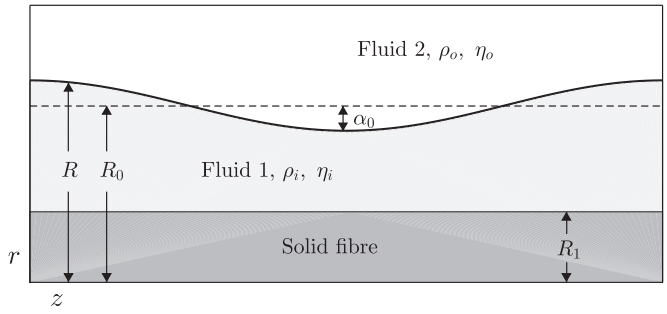

Fig. 2. Schematic of a perturbed cylindrical thread of viscous fluid 1 coating a fibre and embedded in another viscous fluid 2.

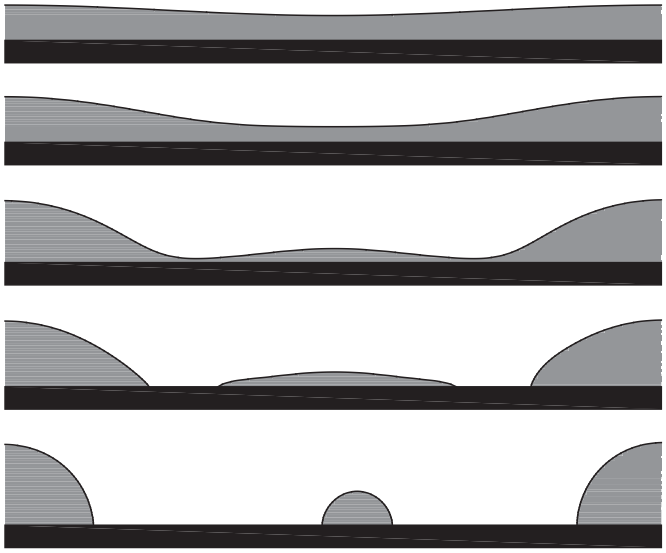

Fig. 3. Temporal evolution of a thread coating a fibre.

$$w_t + uw_r + ww_z = -p_z + \frac{SF^z}{We} + \frac{1}{Re}\left(\frac{1}{r}(r\eta(w_r+u_z))_r + (2\eta w_z)_z\right), \tag{12}$$

$$\phi_t + \frac{1}{r}(r\phi u)_r + (\phi w)_z = \frac{1}{Pe}\left(\frac{1}{r}(r\mu_r)_r + \mu_{zz}\right), \tag{13}$$

$$\mu = \phi^3 - \phi - \epsilon^2\left(\frac{1}{r}(r\phi_r)_r + \phi_{zz}\right), \tag{14}$$

where $u = u(r,z)$ and $w = w(r,z)$ are the radial and the axial velocities, respectively. The subscript index is the differentiation with respect to that index.

3. Numerical solution

Let us consider a two-dimensional axisymmetric computational domain $\Omega = \{(r,z) : R_1 < r < R_2,\ 0 < z < H\}$. We discretize the domain with a uniform mesh spacing h. The center of each cell is positioned at $(r_i, z_k) = (R_1 + (i-0.5)h, (k-0.5)h)$ for $i = 1, \cdots, N_r$ and $k = 1, \cdots, N_z$, where N_r and N_z are the numbers of cells in r and z-directions, respectively. The cell vertices are located at $(r_{i+\frac{1}{2}}, z_{k+\frac{1}{2}}) = (R_1 + ih, kh)$. Given $\mathbf{u}^n = (u^n, w^n)$ and ϕ^n, we want to find $\mathbf{u}^{n+1} = (u^{n+1}, w^{n+1})$ and p^{n+1} which solve the following discrete Eqs. (10)–(12):

$$\frac{1}{r}(ru^{n+1})_r + w_z^{n+1} = 0, \tag{15}$$

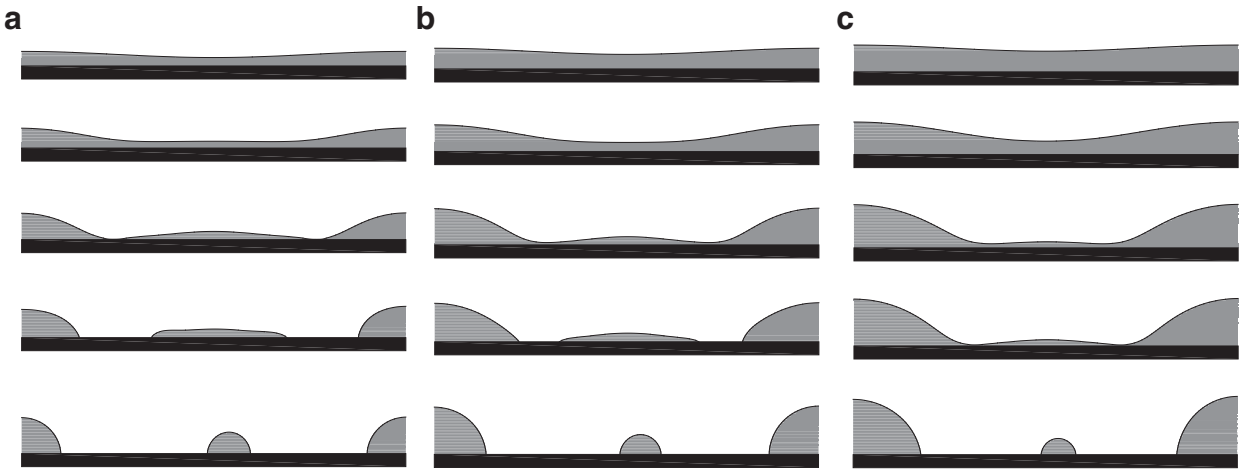

Fig. 4. Temporal evolution of a thread coating a fibre: (a) $R_0 = 0.4$, (b) $R_0 = 0.5$, and (c) $R_0 = 0.6$. The rows from top to bottom are at $t = 0$, 0.2602, 0.4241, 0.4723, and 0.5687.

$$\frac{u^{n+1}-u^n}{\Delta t} = -(uu_r + wu_z)^n - p_r^{n+1} + \frac{SF^r}{We} + \frac{1}{Re}\left(\frac{1}{r}(r(2\eta u_r))_r + (\eta(w_r+u_z))_z - \frac{2\eta u}{r^2}\right)^n, \tag{16}$$

$$\frac{w^{n+1}-w^n}{\Delta t} = -(uw_r + ww_z)^n - p_z^{n+1} + \frac{SF^z}{We} + \frac{1}{Re}\left(\frac{1}{r}(r\eta(w_r+u_z))_r + (2\eta w_z)_z\right)^n. \tag{17}$$

To solve Eqs. (15)–(17), we use the projection method (Chorin, 1997). First, we solve an intermediate velocity field $\tilde{\mathbf{u}} = (\tilde{u}, \tilde{w})$:

$$\tilde{u}_{i+\frac12,k} = u^n_{i+\frac12,k} - \Delta t(uu_r + wu_z)^n_{i+\frac12,k} + \frac{\Delta t}{We}SF^r_{i+\frac12,k} + \frac{\Delta t}{Re}\left(-\frac{2\eta^n_{i+\frac12,k}}{r^2_{i+\frac12}}u^n_{i+\frac12,k} + \frac{2r_{i+1}\eta^n_{i+1,k}\left(u^n_{i+\frac32,k} - u^n_{i+\frac12,k}\right) - 2r_i\eta^n_{ik}\left(u^n_{i+\frac12,k} - u^n_{i-\frac12,k}\right)}{r_{i+\frac12}h^2} + \frac{\eta^n_{i+\frac12,k+\frac12}\left(u^n_{i+\frac12,k+1} - u^n_{i+\frac12,k}\right) - \eta^n_{i+\frac12,k-\frac12}\left(u^n_{i+\frac12,k} - u^n_{i+\frac12,k-1}\right)}{h^2} + \frac{\eta^n_{i+\frac12,k+\frac12}\left(w^n_{i+1,k+\frac12} - w^n_{i,k+\frac12}\right)}{h^2} - \frac{\eta^n_{i+\frac12,k-\frac12}\left(w^n_{i+1,k-\frac12} - w^n_{i,k-\frac12}\right)}{h^2}\right),$$

$$\tilde{w}_{i,k+\frac12} = w^n_{i,k+\frac12} - \Delta t(uw_r + ww_z)^n_{i,k+\frac12} + \frac{\Delta t}{We}SF^z_{i,k+\frac12} + \frac{\Delta t}{Re}\left(\frac{2\eta^n_{i+1,k}\left(w^n_{i,k+\frac32} - w^n_{i,k+\frac12}\right) - 2\eta^n_{ik}\left(w^n_{i,k+\frac12} - w^n_{i,k-\frac12}\right)}{h^2} + \frac{r_{i+\frac12}\eta^n_{i+\frac12,k+\frac12}\left(u^n_{i+\frac12,k+1} - u^n_{i+\frac12,k}\right) - r_{i-\frac12}\eta^n_{i-\frac12,k+\frac12}\left(u^n_{i-\frac12,k+1} - u^n_{i-\frac12,k}\right)}{r_ih^2} + \frac{r_{i+\frac12}\eta^n_{i+\frac12,k+\frac12}\left(w^n_{i+1,k+\frac12} - w^n_{i,k+\frac12}\right) - r_{i-\frac12}\eta^n_{i-\frac12,k+\frac12}\left(w^n_{i,k+\frac12} - w^n_{i-1,k+\frac12}\right)}{r_ih^2}\right),$$

where

$$(uu_r + wu_z)^n_{i+\frac12,k} = u^n_{i+\frac12,k}\bar{u}^n_{r_{i+\frac12,k}} + \frac{w^n_{i,k-\frac12} + w^n_{i+1,k-\frac12} + w^n_{i,k+\frac12} + w^n_{i+1,k+\frac12}}{4}\bar{u}^n_{z_{i+\frac12,k}},$$

$$(uw_r + ww_z)^n_{i,k+\frac12} = w^n_{i,k+\frac12}\bar{w}^n_{z_{i,k+\frac12}} + \frac{u^n_{i-\frac12,k} + u^n_{i-\frac12,k+1} + u^n_{i+\frac12,k} + u^n_{i+\frac12,k+1}}{4}\bar{w}^n_{r_{i,k+\frac12}}.$$

The values $\bar{u}^n_{r_{i+\frac12,k}}$ and $\bar{u}^n_{z_{i+\frac12,k}}$ are defined by the upwind procedure:

$$\bar{u}^n_{r_{i+\frac12,k}} = \begin{cases} \dfrac{u^n_{i+\frac12,k} - u^n_{i-\frac12,k}}{h} & \text{if } u^n_{i+\frac12,k} > 0 \\ \dfrac{u^n_{i+\frac32,k} - u^n_{i+\frac12,k}}{h} & \text{otherwise,} \end{cases}$$

and

$$\bar{u}^n_{z_{i+\frac12,k}} = \begin{cases} \dfrac{u^n_{i+\frac12,k} - u^n_{i+\frac12,k-1}}{h} & \text{if } w^n_{i,k-\frac12} + w^n_{i+1,k-\frac12} + w^n_{i,k+\frac12} + w^n_{i+1,k+\frac12} > 0 \\ \dfrac{u^n_{i+\frac12,k+1} - u^n_{i+\frac12,k}}{h} & \text{otherwise.} \end{cases}$$

The other quantities are similarly defined. At $z = 0$ and $z = H$, symmetric boundary condition is applied. At $r = R_1$ and $r = R_2$, no-slip boundary condition is used. After nondimensionalization, the surface tension term becomes

$$\mathbf{SF} = -\frac{3\sqrt{2}\epsilon}{4}\nabla\cdot\left(\frac{\nabla\phi}{|\nabla\phi|}\right)|\nabla\phi|\nabla\phi.$$

Let the normal vector at $(r_{i+\frac12}, z_{k+\frac12})$ be given by

$$\mathbf{n}_{i+\frac12,k+\frac12} = (n^r_{i+\frac12,k+\frac12}, n^z_{i+\frac12,k+\frac12}) = \left(\frac{\phi_{i+1,k} + \phi_{i+1,k+1} - \phi_{ik} - \phi_{i,k+1}}{2h}, \frac{\phi_{i,k+1} + \phi_{i+1,k+1} - \phi_{ik} - \phi_{i+1,k}}{2h}\right).$$

Then, $\nabla\cdot\left(\frac{\nabla\phi}{|\nabla\phi|}\right)$ is approximated by

$$\nabla_d\cdot\left(\frac{\nabla\phi}{|\nabla\phi|}\right)_{ik} = \frac{1}{2h}\left(\frac{\frac{r_{i+\frac12}}{r_i}n^r_{i+\frac12,k+\frac12} + n^z_{i+\frac12,k+\frac12}}{|\mathbf{n}_{i+\frac12,k+\frac12}|} + \frac{\frac{r_{i+\frac12}}{r_i}n^r_{i+\frac12,k-\frac12} - n^z_{i+\frac12,k-\frac12}}{|\mathbf{n}_{i+\frac12,k-\frac12}|} - \frac{\frac{r_{i-\frac12}}{r_i}n^r_{i-\frac12,k+\frac12} - n^z_{i-\frac12,k+\frac12}}{|\mathbf{n}_{i-\frac12,k+\frac12}|} - \frac{\frac{r_{i-\frac12}}{r_i}n^r_{i-\frac12,k-\frac12} + n^z_{i-\frac12,k-\frac12}}{|\mathbf{n}_{i-\frac12,k-\frac12}|}\right).$$

To avoid division by very small numbers or by zero, we set $\nabla_d \cdot \left(\frac{\nabla\phi}{|\nabla\phi|}\right)_{ik} = 0$ if $|\mathbf{n}_{i+\frac{1}{2},k+\frac{1}{2}}||\mathbf{n}_{i+\frac{1}{2},k-\frac{1}{2}}||\mathbf{n}_{i-\frac{1}{2},k+\frac{1}{2}}||\mathbf{n}_{i-\frac{1}{2},k-\frac{1}{2}}| < 1.0e-12$, which implies the surface tension force is localized in the neighborhood of the interface. The cell-centered normal is $\nabla_d\phi_{ik} = (\mathbf{n}_{i+\frac{1}{2},k+\frac{1}{2}} + \mathbf{n}_{i+\frac{1}{2},k-\frac{1}{2}} + \mathbf{n}_{i-\frac{1}{2},k+\frac{1}{2}} + \mathbf{n}_{i-\frac{1}{2},k-\frac{1}{2}})/4$. When we need surface tension values at edges, we take the average of cell centered values. Next, we solve the following equations for the pressure field:

$$\frac{\mathbf{u}^{n+1} - \tilde{\mathbf{u}}}{\Delta t} = -\nabla_d p^{n+1}, \tag{18}$$

$$\nabla_d \cdot \mathbf{u}^{n+1} = 0, \tag{19}$$

where

$$\nabla_d p^{n+1} = \left(\frac{p_{i+1,k} - p_{ik}}{h}, \frac{p_{i,k+1} - p_{ik}}{h}\right).$$

Note that the first and the second terms of the pressure gradient are stored at $(r_{i+\frac{1}{2}}, z_k)$ and $(r_i, z_{k+\frac{1}{2}})$, respectively. Taking the divergence operator to Eq. (18) and using Eq. (19), we obtain the Poisson equation.

$$\Delta_d p^{n+1} = \frac{\nabla_d \cdot \tilde{\mathbf{u}}}{\Delta t}, \tag{20}$$

where

$$\Delta_d p_{ik}^{n+1} = \frac{r_{i+\frac{1}{2}}(p_{i+1,k}^{n+1} - p_{ik}^{n+1}) - r_{i-\frac{1}{2}}(p_{ik}^{n+1} - p_{i-1,k}^{n+1})}{r_i h^2} + \frac{(p_{i,k+1}^{n+1} - p_{ik}^{n+1}) - (p_{ik}^{n+1} - p_{i,k-1}^{n+1})}{h^2},$$

$$\nabla_d \cdot \tilde{\mathbf{u}}_{ik} = \frac{r_{i+\frac{1}{2}}\tilde{u}_{i+\frac{1}{2},k} - r_{i-\frac{1}{2}}\tilde{u}_{i-\frac{1}{2},k}}{r_i h} + \frac{\tilde{w}_{i,k+\frac{1}{2}} - \tilde{w}_{i,k-\frac{1}{2}}}{h}.$$

We solve Eq. (20) by using a multigrid method (Trottenberg et al., 2001) and the divergence-free velocity is defined by

$$\mathbf{u}^{n+1} = \tilde{\mathbf{u}} - \Delta t \nabla_d p^{n+1}, \text{ i.e.,}$$

$$u_{i+\frac{1}{2},k}^{n+1} = \tilde{u}_{i+\frac{1}{2},k} - \frac{\Delta t}{h}(p_{i+1,k} - p_{ik}),$$

$$w_{i,k+\frac{1}{2}}^{n+1} = \tilde{w}_{i,k+\frac{1}{2}} - \frac{\Delta t}{h}(p_{i,k+1} - p_{ik}).$$

We use a nonlinear gradient stable scheme (Eyre, 1998) for the axisymmetric Cahn–Hilliard equation.

$$\frac{\phi_{ik}^{n+1} - \phi_{ik}^{n}}{\Delta t} = -\frac{r_{i+\frac{1}{2}}(\phi u)_{i+\frac{1}{2},k}^{n} - r_{i-\frac{1}{2}}(\phi u)_{i-\frac{1}{2},k}^{n}}{r_i h} - \frac{(\phi w)_{i,k+\frac{1}{2}}^{n} - (\phi w)_{i,k-\frac{1}{2}}^{n}}{h} + \frac{1}{Pe}\left(\frac{r_{i+\frac{1}{2}}(\mu_{i+1,k}^{n+1} - \mu_{ik}^{n+1}) - r_{i-\frac{1}{2}}(\mu_{ik}^{n+1} - \mu_{i-1,k}^{n+1})}{r_i h^2} + \frac{\mu_{i+1,k}^{n+1} - 2\mu_{ik}^{n+1} + \mu_{i-1,k}^{n+1}}{h^2}\right), \tag{21}$$

$$\mu_{ik}^{n+1} = (\phi_{ik}^{n+1})^3 - \phi_{ik}^{n} - \epsilon^2\left(\frac{r_{i+\frac{1}{2}}(\phi_{i+1,k}^{n+1} - \phi_{ik}^{n+1}) - r_{i-\frac{1}{2}}(\phi_{ik}^{n+1} - \phi_{i-1,k}^{n+1})}{r_i h^2} + \frac{\phi_{i+1,k}^{n+1} - 2\phi_{ik}^{n+1} + \phi_{i-1,k}^{n+1}}{h^2}\right). \tag{22}$$

We apply a nonlinear multigrid method (Kim, 2005b; Trottenberg et al., 2001) to solve the discrete system of Eqs. (21) and (22).

4. Numerical simulations

Before we start, we define the interfacial length parameter ϵ_m as follows:

$$\epsilon_m = \frac{mh}{2\sqrt{2}\tanh^{-1}(0.9)}$$

which implies that we have approximately mh transition layer width (Kim, 2012). For all tests, we use $\epsilon = \epsilon_m$ for some integer m and 90° contact angle boundary condition, unless otherwise specified.

We consider a perturbed cylindrical thread of a viscous fluid 1 coating a fibre, the viscosity and density of which are denoted by η_i and ρ_i respectively, in another viscous fluid 2 of viscosity η_o and density ρ_o. In the unperturbed profile, the interface has a cylindrical shape with radius R_0, see Fig. 2. Typically, the characteristic values of length, viscosity, and density scales are the diameter of a fibre $L_c = 2R_1 = 110\mu m$, $\eta_c = 11 - 23$ poise, and $\rho_c = 0.96\ gcm^{-3}$, respectively, and $0.7L_c < R_0 < 2.125L_c$ (González et al., 2010). The characteristic velocity is defined as $U_c = \sqrt{\sigma_c/(\rho_c L_c)}$ because the flow under consideration is surface tension driven flow.

Fig. 3 shows temporal evolution of a thread coating a fibre. The initial phase field and velocity fields are given by

$$\phi(r, z, 0) = \tanh\left(\frac{R_0 - r + \alpha_0\cos(z)}{\sqrt{2}\epsilon}\right), \tag{23}$$

$$u(r, z, 0) = w(r, z, 0) = 0 \tag{24}$$

on a domain, $\Omega = \{(r, z)|R_1 \le r \le R_1 + \pi \text{ and } 0 \le z \le 2\pi\}$. We use the parameters: $R_0 = 0.5$, $R_1 = 0.2$, $\alpha_0 = 0.05$, $h = \pi/128$, $\Delta t = 0.2h^2$, $\epsilon = \epsilon_4$, $Re = 0.16$, $We = 0.002$, $Pe = 1/\epsilon$, and viscosity ratio $\beta = \eta_i/\eta_0 = 1$. In the following tests, unless otherwise specified, we use Eqs. (23) and (24) as an initial condition and the above parameter values.

4.1. Effect of R_0

We investigate the effect of R_0 on the thread dynamics. The initial conditions are Eqs. (23) and (24). We fix $R_1 = 0.2$. Fig. 4(a)–(c) show the temporal evolution of a thread coating a fibre with $R_0 = 0.4$, $R_0 = 0.5$, and $R_0 = 0.6$, respectively. As R_0 increases, the size of the satellite droplet decreases.

4.2. Effect of R_1

We investigate the effect of R_1 on the thread dynamics. The initial conditions are Eqs. (23) and (24). We fix $R_0 = 0.6$, $Re = 1$ and $We = 0.01$. Fig. 5(a)–(c) show the temporal evolution of a thread coating a fibre with $R_1 = 0.2$, $R_1 = 0.3$, and $R_1 = 0.4$, respectively. As R_1 increases, the size of the satellite droplet decreases.

Next, we highlight the effect of thickness of the fibre R_1 on the breakup of the coating thread. Fig. 6(a) and (b) show the temporal evolution of a thread coating a fibre with $R_1 = 0.4$ and (b) $R_1 = 0.8$, respectively. Here, $R_0 = 0.95$, $Re = 1$ and $We = 0.01$ are used. In the absence of the fibre, if the wave-length of the liquid column is greater than the circumference of the cylinder, then sinusoidal perturbation is unstable (Tomotika, 1935). However, by comparing Fig. 6(a) and (b), we can find that the thick fibre significantly delays the process of Rayleigh instability, i.e., it takes a long time before the liquid undergoes pinch-off.

4.3. Effect of contact angle between solid fibre and liquid

We consider the effect of the surface tension between the solid fibre and the liquid on the interfacial dynamics, which is equivalently the effect of contact angle between the solid fibre and the liquid. Fig. 7 shows the schematic illustration of the contact angle.

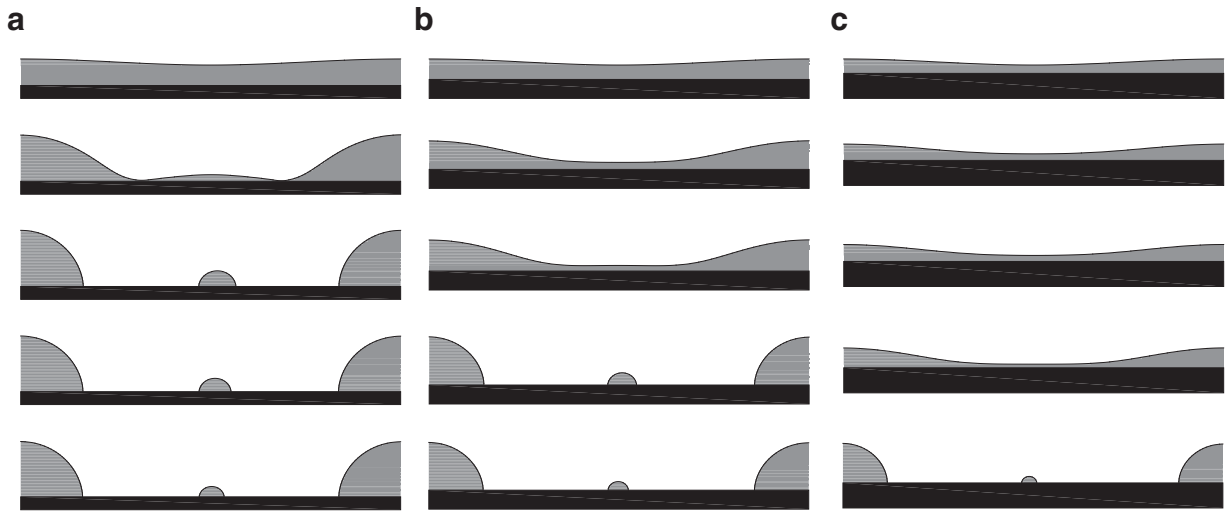

Fig. 5. Temporal evolution of a thread coating a fibre: (a) $R_1 = 0.2$, (b) $R_1 = 0.3$, and (c) $R_1 = 0.4$. The rows from top to bottom are at $t = 0$, 2.1144, 2.6566, 5.3673, and 8.0781.

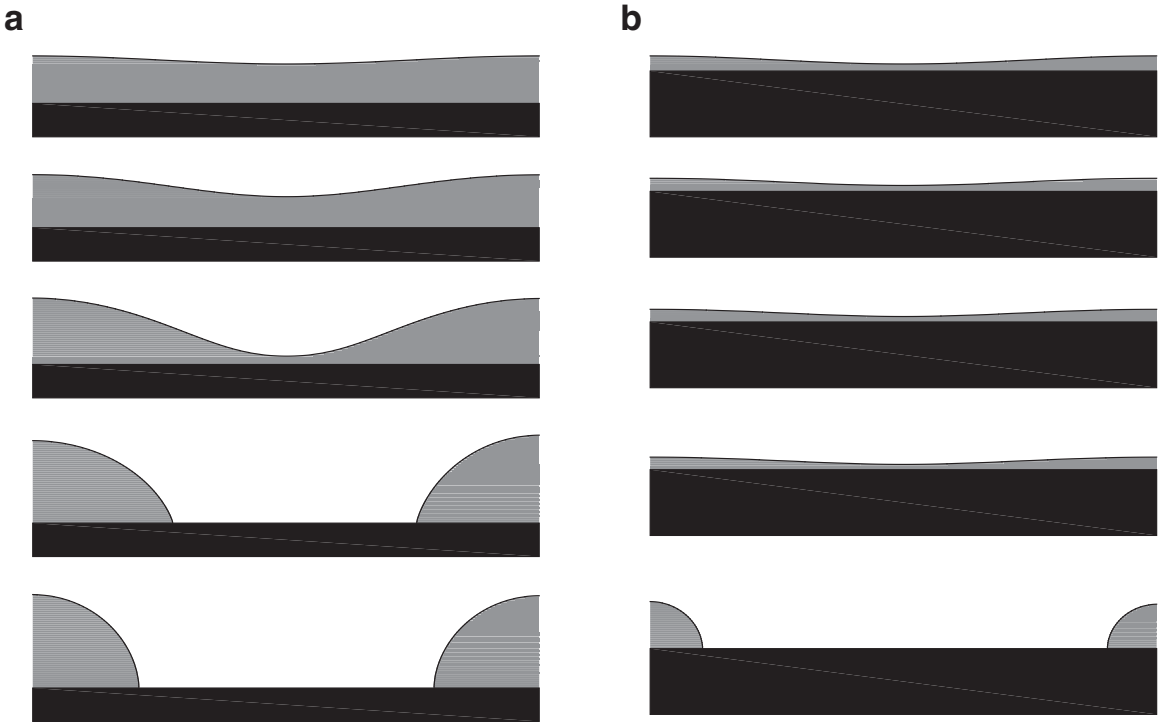

Fig. 6. Temporal evolution of a thread coating a fibre: (a) $R_1 = 0.4$ and (b) $R_1 = 0.8$. Here, $R_0 = 0.95$ is used. The rows from top to bottom are at $t = 0$, 14.3369, 19.1561, 20.6018, and 29.9992.

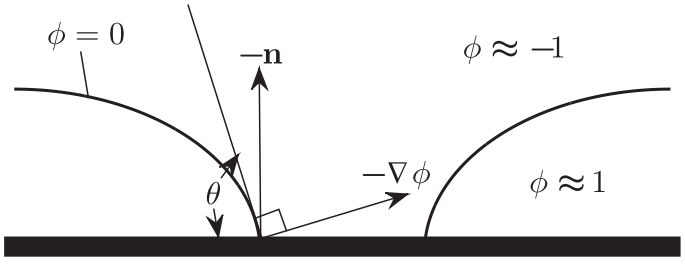

Fig. 7. Schematic illustration of the contact angle.

The contact angle boundary condition on the solid fibre is given as

$$\mathbf{n} \cdot \nabla\phi(r, z, t) = -\frac{G'(\phi(r, z, t))}{\epsilon^2}, \tag{25}$$

where $\mathbf{n}$ is an outer unit normal vector to $\partial\Omega$ and $G(\phi) = \epsilon(\phi^3 - 3\phi)\cos\theta/(3\sqrt{2})$ is the specific wall free energy with the contact angle θ, see Lee and Kim (2011) and references therein for more details about the contact angle boundary condition. At $r = R_1$, the discrete form of Eq. (25) can be written as

$$-\phi_r = -\frac{\phi_{1k} - \phi_{0k}}{h} = -\frac{(\phi_{\frac{1}{2}k}^2 - 1)\cos\theta}{\sqrt{2}\epsilon}, \text{ for } k = 1, \cdots, N_z, \tag{26}$$

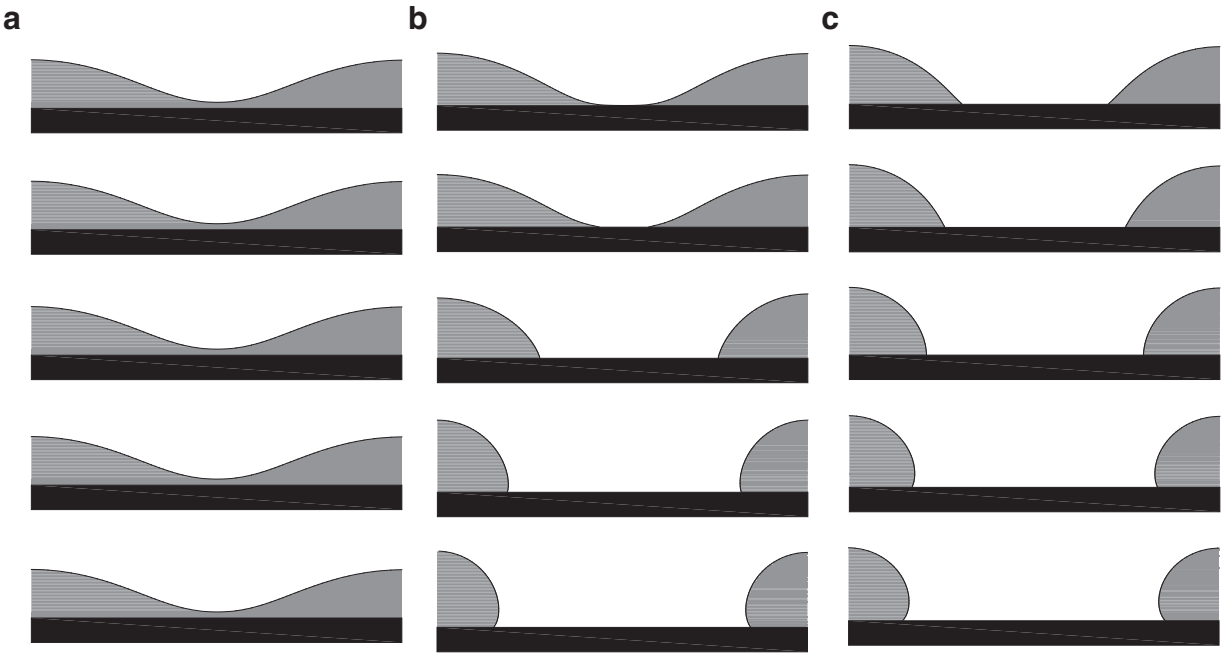

Fig. 8. Temporal evolution of a liquid thread coating a fibre: (a) $t = 19.1561$, (b) $t = 20.6018$, and (c) $t = 36.1436$. The rows from top to bottom are with $30°, 60°, 90°, 120°$, and $150°$ contact angles, respectively.

Then, we can obtain the discrete form of contact angle boundary condition from Eq. (26)

$$\phi_{0k} = \phi_{1k} - \frac{h(\phi_{\frac{1}{2}k}^2 - 1)\cos\theta}{\sqrt{2}\epsilon}, \tag{27}$$

where $\phi_{\frac{1}{2}k} = (3\phi_{1k} - \phi_{2k})/2$. Next, we take the contact angles $30°$, $60°$, $90°$, $120°$, and $150°$ to investigate the effect of contact angle between the liquid and the solid fibre. Here, $R_0 = 0.95$ and $R_1 = 0.4$ are used. From Fig. 8, we can find that the different contact angles between liquid and fibre cause the different temporal evolutions of a liquid thread. As the contact angle increases, it shows the fast dynamics.

5. Conclusion

In this article, we presented a phase-field method for Rayleigh instability on a fibre. The Navier–Stokes–Cahn–Hilliard system was used to model axisymmetric immiscible two-phase flow with surface tension on a fibre. For the numerical solutions, the projection method and the nonlinearly stable splitting method were employed. We presented computational experiments with various thicknesses of liquid thread and fibre. Unlike a liquid column, the evolutionary dynamics of a liquid layer on a fibre depended on the thickness of the fibre. The numerical results indicated that the size of the satellite droplet decreases as the thicknesses of the thread and fibre increase. In upcoming work, we will investigate the effect of the gravitational force on the fluid dynamics on a fibre.

Acknowledgments

The corresponding author (J.S. Kim) was supported by Basic Science Research Program through the National Research Foundation of Korea (NRF) funded by the Ministry of Education (NRF-2016R1D1A1B03933243). The author is grateful to the anonymous referees whose valuable suggestions and comments significantly improved the quality of this paper.

References

Bai, F., He, X., Yang, X., Zhou, R., Wang, C., 2017. Three dimensional phase-field investigation of droplet formation in microfluidic flow focusing devices with experimental validation. Int. J. Multiphase Flow 93, 130–141.
Chakrabarti, T., Verma, N., Manna, S., 2017. Grain boundary driven plateau-rayleigh instability in multilayer nanocrystalline thin film: a phase-field study. Mater. Des. 119, 425–436.
Chorin, A.J., 1997. A numerical method for solving incompressible viscous flow problems. J. Comput. Phys. 135, 118–125.
Eyre, D.J., 1998. Unconditionally gradient stable time marching the cahn–hilliard equation. In: Computational and Mathematical Models of Microstructural Evolution (San Francisco, CA, 1998), Mater. Res. Soc. Sympos. Proc. Warrendale, PA, Vol. 529, pp. 39–46.
González, A.G., Diez, J.A., Gratton, R., Campana, D.M., Saita, F.A., 2010. Instability of a viscous liquid coating a cylindrical fibre. J. Fluid Mech. 651, 117–143.
Gopan, N., Sarith, P.S., 2014. Rayleigh instability at small length scales. Phys. Rev. E. 90 (3). 033001
Haefner, S., Benzaquen, M., Baumchen, O., Salez, T., Peters, R., McGraw, J.D., Jacobs, K., Raphael, E., Dalnoki-Veress, K., 2015. Influence of slip on the plateau-rayleigh instability on a fibre. Nat. Commun. 6 (7409).
Joshi, C., Abinandanan, T., Choudhury, A., 2016. Phase field modelling of rayleigh instabilities in the solid-state. Acta Mater. 109, 286–291.
Kim, J.S., 2005a. A continuous surface tension force formulation for diffuse-interface models. J. Comput. Phys. 204 (2), 784–804.
Kim, J.S., 2005b. A diffuse-interface model for axisymmetric immiscible two-phase flow. Appl. Math. Comput. 160, 589–606.
Kim, J.S., 2012. Phase-field models for multi–component fluid flows. Commun. Comput. Phys. 12, 613–661.
Lamorgese, A., Mauri, R., Sagis, L.M.C., 2017. Modeling soft interface dominated systems: a comparison of phase field and gibbs dividing surface models. Phys. Rep. 675 (6), 1–54.
Lee, H.G., Kim, J.S., 2011. Accurate contact angle boundary conditions for the Cahn–Hilliard equations. Comput. Fluids 44, 178–186.
Lee, H.G., Kim, K.M., Kim, J.S., 2011. On the long time simulation of the Rayleigh–Taylor instability. Int. J. Numer. Methods Eng. 85, 1633–1647.
Müller, T., Sünger, A., Habisreuther, P., Jakobs, T., Trimis, D., Kolb, T., Zarzalis, N., 2016. Simulation of the primary breakup of a high-viscosity liquid jet by a coaxial annular gas flow. Int. J. Multiphase Flow 87, 212–228.
Mead-Hunter, R., King, A.J.C., Mullins, B.J., 2012. Plateau rayleigh instability simulation. Langmuir 28 (17), 6731–6735.
Rodríguez, D., 2017. A combination of parabolized Navier–Stokes equations and level-set method for stratified two-phase internal flow. Int. J. Multiphase Flow 88, 50–62.
Tomotika, S., 1935. On the instability of a cylindrical thread of a viscous liquid surrounded by another viscous fluid. Proc. R. Soc. A 150, 322–327.
Trottenberg, U., Oosterlee, C., Schüller, A., 2001. Multigrid. Academic Press, New York.

Vega, E.J., Montanero, J.M., Herrada, M.A., Ganan-Calvo, A.M., 2010. Global and local instability of flow focusing: the influence of the geometry. Phys. Fluids 22 (6). 064105

Yan, N., Sheng, Y., Liu, H., Zhu, Y., Jiang, W., 2015. Templated self-assembly of block copolymers and morphology transformation driven by the Rayleigh instability. Langmuir 31 (5), 1660–1669.